Title: Neural codes for visual numerosity independent of other quantities are present both in the dorsal and in the ventral stream of the human brain

Author names and affiliations: Alireza Karami1, Elisa Castaldi2, Evelyn Eger3, and Manuela Piazza1

1 Center for Mind/Brain Science, University of Trento, 39068 Rovereto, Italy
2 Department of Neuroscience, Psychology, Pharmacology and Child Health, University of Florence, Florence, 50135, Italy
3 Cognitive Neuroimaging Unit, CEA DRF/Joliot, INSERM, Université Paris-Saclay, NeuroSpin Center, 91191 Gif-sur-Yvette, France

Corresponding authors email address: Alireza Karami (alireza.kr@gmail.com), Manuela Piazza (manuela.piazza@unitn.it)

Abstract

Representing the number of items in sets (numerosity) is a core and evolutionary ancient ability. In a recent fMRI study Castaldi et al. (eLife 2019) showed that visual numerosity is represented independently from other visual features starting from early visual areas and progressively amplified along the dorsal stream hierarchy up to parietal areas. However, because in this study we recorded the brain activity from a restricted brain volume, and performed the analyses only in a series of retinotopically organized regions of interest along the dorsal stream, we still miss an exhaustive picture of the full network of regions encoding pure numerosity across the whole brain. In this research advance, we extend the findings of Castaldi et al. in two significant ways. First, we recorded the whole brain which allowed us to characterize the neural responses to numerosity beyond the dorsal stream using a searchlight analysis in addition to an ROIs approach. Second, in addition to the classical model-based analytical approach, such as RSA, we compared the neural representational geometries across the different regions using multi-dimensional scaling, an hypothesis-free approach capable of unveiling latent neural dimensions that might otherwise go unnoticed. Our results confirm that numerosity is represented over and above other visual features in early visual areas and progressively enhanced in associative areas of the dorsal stream but also, notably, of the ventral stream. We also found that numerosity representations in association areas differ substantially from those of early visual areas, and that in associative regions of both streams numerosity is represented on a similar manifold akin to a curved number line, a structure suggestive of their similar involvement in numerosity-based decision making. Taken together, these results call for an important revision of the existing neurocognitive models of number cognition.

Impact statement

Visual numerosity is represented in associative areas of dorsal and ventral streams on a neural manifold that also reflects decision variables, suggesting a common role in numerosity decision-making.

Keywords

Numerosity, Dorsal Stream, Ventral Stream, Representational Similarity Analysis, Multidimensional Scaling

Introduction

The ability to estimate the number of objects (numerosity) in the environment is ontogenetically precocious and phylogenetically ancient. In animals it is of high adaptive value (Nieder, 2020). In humans it also plays an additional role in scaffolding the acquisitions of symbolic numeracy (Piazza, 2010; Halberda et al., 2008; Decarli et al., 2023), representing a potential target for math education and remediation. Single cell recording studies indicate that in both in the animal (e.g., Nieder & Miller, 2003; Wagener et al., 2018; Kobylkov et al., 2022) and the human brain (Kutter et al., 2018) there are numerosity-tuned neurons, whose Gaussian tuning functions reflect scalar variability and whose activity underlies behavior in numerosity comparison and matching tasks, similarly adhering to Weber's law (Gallistel & Gelman, 1992; Merten & Nieder, 2009; Ditz & Nieder, 2016; Piantadosi & Cantlon, 2017). This approximate and compressed code can also be inferred from the population-level responses to numerosity as measured by fMRI using multivariate pattern analyses, adaptation, or population receptive field mapping approaches (e.g., Piazza et al., 2004; Eger et al., 2009; Harvey et al., 2013). However, because numerosity is necessarily coupled with other visual characteristics of the sets (e.g., more items tend to occupy a larger area, or to be more densely spaced), establishing the degree to which the observed neural response to numerosity is distinct from the response to other visual attributes is not trivial. To address this issue Castaldi et al. (2019) recently analyzed the human BOLD response to numerosity combining multivariate analyses with multiple regression, allowing the estimation of the brain activity evoked by different numerosities once taking into account the effects of other relevant non-numerical variables at the same time (Castaldi et al., 2019). This study however solely focussed on the dorsal stream and demonstrated that numerosity is represented over and above other visual features in retinotopic regions of interest and that, especially when task relevant, it is amplified in parietal areas. In terms of localization, these results were in agreement with several previous observations, including the first single cell recordings in macaques (Nieder & Miller, 2003; Nieder & Miller, 2004) and the first fMRI studies in humans (e.g., Piazza et al., 2004; Cantlon et al., 2006; Castelli et al., 2006; Ansari & Dhital, 2006) that suggested that parietal cortex is the key brain region for numerosity processing (see for a review: Eger, 2016; Faye et al., 2019). They were

also consistent with the neuropsychological literature that associates deficits in numerosity processing to parietal cortex damage (Warrington & James, 1967; Lemer et al., 2003). Partially biased by these initial observations, several later key fMRI studies on numerosity restricted the brain data acquisition to a limited volume centered on parietal cortex (e.g. Eger et al., 2009; Castaldi et al., 2019) or focussed the analyses on parietal cortex using an ROI approach (e.g., Bulthè et al., 2015; Castaldi et al., 2020). While a few studies looking at the whole brain did sometimes report numerosity-related response outside parietal cortex, both in the frontal and in the occipito-temporal cortex (e.g., Bulthè et al., 2014; Harvey & Dumoulin, 2017), they mostly tested small numerosities, which some suggest are elaborated by a dedicated mechanism, referred to as “subitizing”, potentially different from the one at play with large numerosities (Revkin et al., 2008; Kutter et al., 2023). A notable exception is the recent work of Cai et al. (2021), who employed a population receptive field mapping (pRF) method (Harvey & Dumoulin, 2017) and found that the numerotopic maps that encode small numerosities in the dorsal and ventral stream also respond to large numerosities. A couple of important limitations from this study, however, call for further confirmations for this stand-alone report:

1) In the study there was no attempt at controlling /analyzing the impact of non-numerical features. In all stimuli total surface area was held constant across numerosities, thus as a consequence dot size decreased and density increased with number. This prevents concluding that the activation to numerosity was solely due to numerosity and not to concurrent changes in other visual features.

2) The strictly ordered presentation of numerosities (ascending or descending), while ideal for pRF approach, likely created expectations and attentional biases, the effect of which cannot be readily disentangled from the effect of numerosity itself.

Thus, the question of whether large numerosity is encoded over and above the other visual properties solely along the dorsal stream, or whether it is also represented in other regions of the human brain still remains open. In order to probe this questions, here we adapted the paradigm of Castaldi et al. (2019) and recorded the BOLD signal from the whole brain of subjects looking at sets of different number of dots, and analyzed the data using a combination of model-based representational similarity and dimensionality reduction analyses, both in pre-defined ROIs and across the whole brain.

Materials and Methods

Participants

Thirty-seven healthy adults (twenty-two females; mean age 21.9 years) with normal or corrected vision participated in the study. The ethics committee of the University of Trento (Italy) approved the study, and all participants gave written informed consent and were reimbursed for their time. Given their excessive head motion (translation, in one of the directions x,y or z, greater than 3mm, or rotation, around one of the axes, greater than 2 degrees) or poor behavioral performance (accuracy < 65%), data from six participants (four for poor behavioral performance and two for excessive head motion) were excluded from the final analysis. This led to the final sample of thirty-one subjects (eighteen females; mean age 21.9 years).

Experimental Design and Statistical Analyses

Stimuli and procedure

Participants were familiarized with the task by practicing 20 trials outside of the MRI before the experiment. During fMRI scanning, arrays of black dots on a mid-gray background were centrally shown to participants. Dots orthogonally varied in number, average item area, and total field area (similar to Castaldi et al., 2019). There were 32 conditions (resulting by crossing 4 numerosities, 4 average item areas, and 2 total field areas): six, ten, seventeen, or twenty-nine dots were presented with varying average item area (0.04, 0.07, 0.12, 0.2 visual square degree) that were made to fit within a small or large total field area (defined by a virtual circle of either about 9 or 13.5 visual degree diameter; Figure 1.A). Numbers and average item areas were chosen based on previous behavioral studies (Castaldi et al., 2018; Castaldi et al., 2019) to be equally discriminable. Total field areas were selected to have suitably sparse arrays of dots (1 dot/vd^2) to be within the numerosity estimation and not the density estimation regime (Anobile et al., 2013).
In each trial, a set of dots was presented for 500 ms over a wide thin red fixation cross, and participants were required to estimate their number and keep them in memory until, after a variable ISI of 3.5–5.5 s, the next set of dots appeared (Figure

1.B). When the color of the fixation cross changed from red to green, subjects were required to compare the number of dots in the current set (match stimulus) with the previous one and determine whether it was larger or smaller by pressing one of two buttons following the instructions. After a button press, the background cross turned red again, and a variable blank delay of 3.5–5.5 s preceded the following trial. Match stimuli were designed to be ~2 JNDs larger or smaller in numerosity than the previous sample stimulus, based on an average numerosity Weber fraction estimated on an independent group of healthy adults (Castaldi et al., 2018), while the other dimensions (total field area and average item area) were the same. Match trials occurred ~20% of the time.

The experiment consisted of six runs, with two blocks within each run. Each block consisted of thirty-six trials: four match trials and thirty-two sample trials, one for each condition (4 number × 4 average item area × 2 total field area). After the third run, in the middle of the experiment, participants' hand-response correspondence was switched. There was a brief practice session at the beginning of the experiment and after changing the hand assignment. Each run lasted ~7 minutes.

fMRI recordings and preprocessing

Functional images were acquired at the Center for Mind/Brain Sciences (CIMeC) with a SIEMENS MAGNETOM PRISMA 3T with gradient insert of 80mT/m max and using a SIEMENS Head/Neck 64-channel phased array coil. Visual stimuli were presented through a mirror system connected to a 42″ LCD monitor (MR-compatible, Nordic NeuroLab) positioned at the back of the magnet bore. Functional images were acquired using echo-planar (EPI) T2*-weighted fat-saturation echo-planar image (EPI) volumes with 1.75 mm isotropic voxels using a multi-band sequence (Moeller et al., 2010) (https://www.cmrr.umn.edu/multiband/, multi-band [MB] = 3, GRAPPA acceleration with [IPAT] = 1, partial Fourier [PF] = 7/8, matrix = 120×120, repetition time [TR] = 20.3 ms, echo time [TE] = 31.2 ms, echo spacing [ES] = 0.62 ms, flip angle [FA] = 60°, bandwidth [BW] = 2450 Hz/px, phase-encode direction Anterior >> Posterior). In total, 1206 volumes from the six experimental runs made up the functional acquisition. A whole-brain gradient echo B0 map, matched for spatial resolution, was acquired after the functional scans for fieldmap-based correction of susceptibility-induced geometric distortions. T1-weighted anatomical

images were acquired at 1 mm isotropic resolution using an MPRAGE sequence (GRAPPA acceleration with [IPAT] = 2, matrix = 176×256, repetition time [TR] = 2530 s, echo time [TE] = 1.69 ms, time of inversion [TI] = 1100 ms, flip angle [FA] = 7°, bandwidth [BW] = 650 Hz/px). Padding and tape were used to reduce head movement. In their left and right hands, participants held two response buttons. Stimuli were presented using a custom-written Psychtoolbox 3 (Brainard, 1997) script running in MATLAB R2018 (The MathWorks, Inc., Natick, MA).

Functional images were preprocessed in MATLAB R2019 using the Statistical Parametric Mapping Software (SPM12, https://www.fil.ion.ucl.ac.uk/spm/software/spm12/). Preprocessing included the following steps: Slice-time correction of functional images to the middle slice, applying distortion correction to all functional images, realignment of each scan to the mean of each run, co-registration of the anatomical scan to the mean functional image, and segmentation of the anatomical image into native space tissue components.

The preprocessed EPI images (in subjects' native space) were high-pass filtered at 128 s and pre-whitened by means of an autoregressive model AR(1). A general linear model (GLM) was used to estimate subject-specific beta weights. For each run, thirty-two regressors of interest were included for all sample stimuli (4 number × 4 average item area × 2 total field area). Regressors for match stimuli, left hand, and right hand were also included. Nuisance regressors were identified with The PhysIO toolbox (Kasper et al., 2017) using six motion parameters and CompCor with five components (Behzadi et al., 2007) and were included in the GLM.

The surface of each subject was generated using Freesurfer 6 (https://surfer.nmr.mgh.harvard.edu/) (Fischl, 2012). The surfaces were then converted to a SUMA standard mesh of 141,000 nodes per hemisphere (Saad et al., 2004) from each participant's anatomical scan using algorithms implemented in the Surfing toolbox (https://surfing.sourceforge.net) (Oosterhof et al., 2011) to produce node-to-node anatomical correspondence across participants' surfaces. For each subject, the parameter estimates (beta weights) for each of the 32 regressors of interest were converted into a t-statistic and projected on the SUMA standard mesh using AFNI's 3dVol2Surf (https://afni.nimh.nih.gov/) (Cox, 1996) with the "average" mapping algorithm, which roughly represents the value at each vertex of the surface

as the average value along a line connecting the smooth white matter and pial surfaces.

fMRI data analysis

First, in order to visualize the brain regions with activation during the stimuli, we smoothed with a Gaussian 4 mm FWHM filter using the SurfSmooth function with the HEAT_07 smoothing method the contrast map of sample stimulus against the implicit baseline (Chung et al., 2005). We then performed a surface-based random-effects group analysis using a one-sample t-test. The result was then corrected using threshold-free cluster enhancement (TFCE; Smith & Nichols, 2009) using Monte Carlo simulations with 10,000 permutations, as implemented in the CoSMoMVPA MATLAB toolbox (Oosterhof et al., 2016) and projected onto the fsaverage surface for visualization (thresholded at $p < 0.01$, one-tailed).

Second, in order to test if and in which brain regions the representations of numerical and the non-numerical features could be dissociated, we used Representational Similarity Analysis (RSA; Kriegeskorte et al., 2008; Kriegeskorte & Kievit, 2013) which allows to assess the effects of the experimental conditions on distributed activity patterns. We adopted two approaches: a Region Of Interest (ROI) and a whole brain searchlight approach (see below). In both cases we used the t-statistics from the first-level analysis to extract the neural representational dissimilarity matrix (RDM) by computing the correlation distance (Pearson correlation) between activation patterns for each pair of conditions. Each pattern underwent voxel-wise scaling by demeaning the data across conditions before computing the correlation. We then applied semipartial correlation (Pearson correlation) analysis to test if and to what extent the fMRI pattern dissimilarity structure could be explained by multiple predictor matrices reflecting the stimuli's dissimilarity along several quantitative dimensions: numerosity, average item area, total field area, total surface area and density. Note that our design orthogonally manipulated numerosity, average item area and total field area. As a result, numerosity was partly correlated with density and total surface area (correlation between number and density predictor matrix = 0.84; between number and total surface area predictor matrix = 0.36). In order to control the potential impact of shared variance among our predictor variables and to ensure a more accurate assessment of each variable's contribution, we employed

semipartial correlation analysis (Abdi 2007). This statistical technique allowed us to disentangle the unique influence of each predictor variable from the common variance they share, thereby preventing an overestimation of their individual effects due to repetitive inclusion of shared components in our analysis. Thus, the coefficient of semipartial correlation between the neural RDM and the model RDM of interest represents the portion of unique variance shared between the neural RDM and the model RDM of interest while partialling out the effect of all other models. A schematic representation of this process is shown in Figure 2. To account for different levels of noise in different brain areas, we estimated the noise ceiling in all ROIs and normalized the semipartial correlation coefficients with the corresponding noise ceiling (Khaligh-Razavi et al., 2018; Al-Tahan & Mohsenzadeh, 2021). The noise ceiling was determined by correlating the mean across individual participant's RDM and the group-averaged RDM (Nili et al., 2014).

Surface-based ROI RSA

Following Castaldi et al. (2019), we selected several retinotopic regions of interest (ROIs) along the dorsal stream from a surface-based probabilistic atlas based on visual topography, averaging across the two hemispheres (Wang et al., 2015). Moreover, because contrary to Castaldi et al. (2019) we recorded from the whole brain, we extended the analysis to the retinotopic regions of the ventral stream as defined by the same atlas (Wang et al., 2015). The ROIs in early visual areas were V1, V2 and V3. The ROIs along the dorsal stream were V3AB (merging V3A and V3B), V7, IPS12 (merging IPS1 and 2), IPS345 (merging IPS3, 4 and 5; Figure 3.A). These were further merged into two large ROIs that correspond to intermediate (V3A, V3B, and V7, also known as IPS0), and higher-level (IPS1 to IPS5) areas. The selected ROIs from the ventral stream were hV4, VO1, VO2, PHC1, PHC2 (Figure 3.B). The ventral ROIs were also further merged into two large intermediate (VO1 and VO2), and higher-level (PHC1 and PHC2) ROIs. In order to ease comparisons between ROIs we performed the subsequent analyses based on the 600 most active vertices (in the contrast “all sample stimuli > baseline”) in all ROIs (Mitchell et al., 2004). We choose the vertices from each individual ROI and large ROI separately. The number of vertices (600) was chosen to be slightly lower than the maximum number of vertices across all ROIs (ranging from 661 to 1510). It is important to note,

though, that when we selected all vertices across each ROI the results remained substantially unchanged. For the ROI RSA we used unsmoothed data but the results remained consistent when we smoothed the data. ROI-based RSA was implemented using the CoSMoMVPA MATLAB toolbox (Oosterhof et al., 2016) and custom-written code in MATLAB R2019. We used one-sample t-tests against zero across subjects to test the statistical significance of the Fisher-transformed semipartial correlation coefficients for each feature and ROI. We analyzed the effects of ROI and features with repeated measures analysis of variance (ANOVA).

Surface-based searchlight RSA

To find how numerical and non-numerical quantities are represented across the whole cortical surface, RSA was performed using a surface-based searchlight approach (Oosterhof et al., 2011), implemented using the CoSMoMVPA MATLAB toolbox (Oosterhof et al., 2016), the Surfing toolbox (Oosterhof et al., 2011), and a custom-written code in MATLAB R2019 (The MathWorks, Inc., Natick, MA). Each participant's entire t-statistics brain map was smoothed with the same method we used to smooth the contrast map and underwent a searchlight (radius 6 mm along the cortical surface) procedure. A neural RDM was constructed using Pearson's correlation. Similar to the ROI-based RSA, the semipartial correlation between the neural RDM and model RDMs were calculated and then mapped on the brain.
To identify vertices in which the Fisher-transformed semipartial correlation resulting from searchlight RSA was significantly above zero, a one-sample t-test was used across subjects. The result was then corrected using threshold-free cluster enhancement (TFCE; Smith & Nichols, 2009) using Monte Carlo simulations with 10,000 permutations implemented in the CoSMoMVPA MATLAB toolbox (Oosterhof et al., 2016). The resulting statistical map was thresholded at $p < 0.01$ (one-tailed) and was projected on the fsaverage surface for visualization.

Multidimensional scaling

The results from RSA show how each feature contributes to the variance in our data, in a hypothesis-driven manner. To further explore the latent structure of our neural data we complemented RSA with a data-driven approach, implementing multidimensional scaling (MDS; Kruskal, 1964) using the MATLAB function

cmdscale. MDS spatially organizes the stimuli so that their relative distance mirrors the differences in the brain activity patterns they evoke. We used MDS and visualized the first two dimensions to investigate the neural representational geometry of our stimuli space both across and within ROIs. To compare the similarity of the neural representation of the stimulus space across ROIs, we vectorized the 32 x 32 neural RDM reflecting the correlation across conditions within each of the 12 ROIs and then constructed a 12 × 12 RDM across ROI. Then, to further explore the neural representational geometry within each stream, we applied the MDS on the group-average RDM across participants for each ROI. We also extended these analyses beyond the dorsal and ventral retinotopic regions including three additional clusters resulting from the whole brain searchlight map of regions encoding numerosity. To isolate these clusters we used group-constrained subject-specific (GCSS) analyses (Fedorenko et al., 2010; Julian et al., 2012), using custom-written MATLAB R2019 code (The MathWorks, Inc., Natick, MA) developed by Scott & Perrachione (2019; available at https://github.com/tlscott/make_parcels). The identification of these clusters involved a four-step process: Initially, for each participant, the Fisher-transformed semipartial correlation values resulting from the number searchlight maps were converted into z-scores. Subsequently, these z-scores were thresholded at $p < 0.01$ and binarized. Secondly, a probability map was generated by overlaying all binary maps. This resulting map was smoothed using a gaussian kernel of 6 mm FWHM, and vertices with contributions from fewer than ten subjects were set to zero. Thirdly, the watershed algorithm, as implemented in the SPM-SS toolbox (Nieto-Castañón & Fedorenko, 2012; https://www.nitrc.org/projects/spm_ss), was employed to locate local maxima. Clusters were defined around these local maxima and extended to neighboring vertices until a local minimum or a zero-valued vertex was encountered. The resulting parcels represent regions where multiple subjects exhibited suprathreshold activity, without the requirement that this activity occur in the exact same vertex across participants. Finally, the number of subjects contributing to each parcel was calculated, and parcels where more than 80% of subjects contributed were selected as the final parcels (Scott & Perrachione, 2019).

Code accessibility

All the code related to this study is available through GitHub: https://github.com/alireza-kr/numerosity_fmri-meg-cnn/

Results

Thirty-one healthy adult volunteers completed a numerosity comparison task on arrays of dots orthogonally varying in numbers of items (6, 10, 17, 29), average item areas (0.04, 0.07, 0.12, 0.2 visual squares degree), and total field areas (9 or 13.5 visual degree diameter) while being scanned in a 3T MRI. Their task was to keep the number of dots from the sample stimulus in their memory to compare it with an occasionally presented subsequent match stimulus. Behavioral performance on this numerosity comparison task was overall high (Mean=82.14%, SD=6.83%, Range=66.66% – 93.75%), indicating that subjects were attentive.

Univariate fMRI activation

We started the analysis of the functional imaging data by evaluating the overall regional activation during the experiment. Surface-based random-effects group analysis for sample stimulus against the implicit baseline revealed activation across both hemispheres in a wide set of regions extending both dorsally from early visual to parietal up to the postcentral gyrus and the precentral sulcus in the frontal cortex and ventrally including medial and lateral inferior occipito-temporal areas (Figure 1.C, thresholded at $p < 0.01$, TFCE corrected).

ROI semipartial correlation RSA

Following Castaldi et al. (2019), to disentangle the contribution of numerical and non-numerical features of the stimuli on the distributed patterns of activity of the BOLD signal, we performed RSA (Kriegeskorte et al., 2008) using semipartial correlation, which ensures that the resulting coefficients reflect the unique variance explained by each model while partialling out the effect of all other models. We performed this analysis on 12 ROIs derived from a surface-based probabilistic atlas based on visual topography (Wang et al., 2015): 3 in early visual areas (V1, V2, V3), 4 along the dorsal stream (V3AB, V7, IPS12, IPS345), and 5 along the ventral

stream (hV4, VO1, VO2, PHC1, PHC2). The results indicate that the variance in brain activation patterns was significantly explained by number over and above all other non-numerical features in almost all regions (except V3 and PCH2, all $p<0.01$) starting in early visual areas and reaching its highest explanatory power in higher-level regions V7-IPS along the dorsal stream and VO1-VO2 along the ventral stream. An opposite pattern of results was seen for most non-numerical features that were maximally represented in early visual areas: total field area explained independent portions of variance in all regions, but maximally in V1-V3 and less so in higher-level regions of both streams; total surface area was significant only up to V3AB and hV4; density also was significant in V1-V3 and hV4, then ceased to explain a significant portion of the variance but regain some effect in IPS1-5. Average item area, instead, was never significant, neither in the dorsal nor in the ventral stream regions (Figure 3.C and 3.D).

To statistically evaluate the impact of the different features across the ROIs, we analyzed the semipartial correlation coefficients with four repeated measures ANOVAs (see below) with ROIs and features as factors. ROIs were considered both aggregated in three big regions, and separately for each of the individual regions, for the ventral and the dorsal stream separately. The significant two-way interaction between ROIs and features that we observed in all the 4 ANOVAs confirmed that the five features were differently encoded across ROIs across both the dorsal (for the three large regions: $F(4.30,128.95)=36.680$, $p<0.001$; for the individual seven regions: $F(8.10, 243.08)=32.404$, $p<0.001$) and the ventral stream hierarchy (for the three large regions: $F(3.56, 106.91)=29.330$, $p<0.001$; for the individual eight regions: $F(9.56, 286.82)=27.513$, $p<0.001$).

We then performed five one-way repeated measures ANOVAs on each feature across the ROIs. They revealed that, with the exception of average item area, the features were encoded differently across ROIs along both streams (main effects of ROIs: $p<0.01$ for dorsal regions and $p<0.01$ for ventral regions, for both aggregated and individual ROIs)(average item area: three large ventral regions: $F(1.91,57.40)=2.304$, $p=0.111$; eight individual ventral regions: $F(5.45,163.43)=1.362$, $p=0.238$). Finally, one-way repeated measures ANOVA on both individual ROIs and merged ROIs showed a main effect of features (all $p<0.01$). Taken together these results indicate that numerosity is represented independently from other visual features along both dorsal and ventral retinotopic regions and that

contrary to all other features it is amplified in associative areas (IPS and VO) in both streams (linear regression of the semipartial correlation coefficient of number from V1 to IPS (β=0.02, $p<0.00$); and from V1 to VO (β=0.02, $p<0.00$).

Searchlight semipartial correlation RSA

We then investigated how patterns of activity are captured by models representing numerical and non-numerical feature dissimilarity across the entire cortical surface through a surface-based searchlight RSA. Results revealed that numerosity explained variance in several regions widely spread across the cortical surface (Figure 4), extending well beyond the previously defined retinotopic ROIs. These regions include the mid and anterior parietal cortex, both superior, inferior, and anterior to the intraparietal sulcus, the parieto-occipital cortex, the precentral gyrus and superior frontal sulcus. Along the ventral stream, the regions isolated through the searchlight that were not already part of the previously considered retinotopic ROI areas extended laterally in the mid inferior temporal lobe. With respect to previously described functional parcellations of the ventral stream, our large ventral numerosity-related region appears to overlap with the “number form area” (see Yeo et al., 2017), but also to extend further and include the “visual word form area-1”, the “fusiform face area” and the “fusiform body area”, as defined by the functional atlas by Rosenke and colleagues (Rosenke et al., 2020). Thus, numerosity is also encoded in non topographically organized areas in the parietal, occipito-temporal, as well as in the frontal lobes. On the contrary, all non-numerical features (apart from average item area, for which we could not find any regions representing it) explained variance mainly in the early visual cortex (Figure 4).

The neural representational geometry across regions

To further explore whether the neural representational geometry of our stimulus space was similar or differed across regions and especially across streams, we used multidimensional scaling (MDS), a data-driven approach that recovers a low-dimensional representation of the neural similarity structure. We applied MDS both across ROIs and across stimulus conditions within ROIs.
The across topographically organized ROIs MDS (Figure 5.A) identified three clusters of ROIs: one grouping together early visual regions, the other all ventral

regions, and the third one all the dorsal regions, suggesting that the three groups of regions represent the stimulus space differently. This result prompted us to further investigate the neural representational geometry of each ROI separately (see figure 5.B). The results indicate an ordered representation of numerosity along both main dimensions of the stimulus space, as well as a clear separation between stimuli with large and small total field area in the early visual areas. While this pattern remains approximately constant along the ventral stream ROIs up to VO2, it changes as we get to the higher ROIs along the dorsal stream (IPS12 and IPS345): here the separation based on total field area decreases and a curved pattern around the midpoints representing number emerges. This curved pattern is not evident in the ventral stream areas VO1 and VO2. Interestingly, the RSA semipartial correlation analysis indicated an equally significant representation of numerosity in VO1, VO2, and V7, IPS12, and IPS345. Thus, even though numerosity information is equally present in retinotopic areas of both streams, the underlying geometry differs between streams.

Importantly, however, this difference disappears when focusing on regions outside the retinotopic ROIs. The GCSS procedure used to identify those regions yielded several parcels along both streams, which we grouped as follows: within the dorsal stream the parcels were 8: three in the right and five in the left hemisphere, and we grouped them into two bilateral groups, one more posterior and one more anterior. We called these NPC (as in Numerosity Parietal Cortex) 1 and 2 , using the Harvey & Dumoulin's (2017) name convention because of the similarity in localization with their study.

The ventral parcels were 6, three per hemisphere, and they were considered as one group which was labeled "NTO" (as in Numerosity Temporo-Occipital), due to the apparent overlap with the NTO region described by the same authors. The MNI coordinates of our ventral parcels were [46, -71, -6; 46, -67, 3; 47, -60, -6; -46, -62, -6; -48, -79, -11; -44, -61, -13].

All three macro regions (the ventral area NTO and the parietal NPC1 and NPC2) responded to numerosity with a similar curved structure (Figure 6), indicating a similar representational pattern, in sharp contrast with that recovered in early visual areas.

Discussion

The present study used RSA and MDS to investigate whether, where and how the human adult brain represents numerosity and other visual features of sets using fMRI and a numerosity estimation task.

The ROI and searchlight RSA showed that numerosity and the other visual properties of sets (with the notable exception of average item area, which we did not find to be encoded in any region) are represented independently from one-another in several brain regions, consistent with the existence of partially independent channels (congruent with Castaldi et al., 2019). However, while the representations of the non-numerical visual features, such as total field area, total surface area, and density, tend to remain confined to early visual areas, the representation of numerosity is present more widely across the cortex, far exceeding the retinotopic regions, and amplified in association areas. Importantly, we found that large numerosity representations are not only present along the dorsal stream, as often previously reported in the literature (with the notable exception of Cai et al., 2021, who nevertheless did not control for the non-numerical features of the stimuli), but also along the ventral visual stream of both hemispheres. Starting from early visual regions (V1-V3) numerosity is progressively amplified both within and outside retinotopic regions along both streams, extending both anterior, superior, and inferior to the IPS, and both anterior and lateral to the occipito-temporal areas VO. The fact that numerosity-related responses along the ventral stream were seldom reported in the previous neuroimaging literature could be explained by the fact that, due to prior biases towards parietal cortex, some only scanned a limited brain volume centered on the parietal lobe (e.g., Lasne et al., 2019; Castaldi et al., 2019); others, while recording the whole brain, often focused their analyses on parietal cortex regions (e.g., Bulthè et al., 2015); others, finally, may have been limited in their power to detect such ventral activation due to the use of passive or minimally demanding tasks (e.g., Piazza et al., 2004). However, also in light of the neuropsychological literature that consistently associates deficits in numerosity processing to parietal cortex damage (Warrington & James, 1967; Lemer et al., 2003), our report of a robust response to numerosity in occipito-temporal regions remains surprising. We think of two possible interpretations of this result: the first one sees the representation of numerosity in the ventral stream as the result of formal math

education and of the functional connectivity between this region and the parietal regions (Kay & Yeatman, 2017; Conrad et al., 2022). This view stems from two observations: 1) young children are endowed with a precocious sense of numerosity that seems to mainly emerge from a parietal cortex circuit (Cantlon et al., 2006; Izard et al., 2008; Hyde et al., 2010), 2) during math education a specific portion of the ventral visual stream functionally specializes in the recognition of digits, giving rise to the Number Form Area (NFA; Amalric & Dehaene, 2016; Grotheer et al. 2018; Kersey et al., 2019; Kutter et al., 2022; see for a review: Yeo et al., 2017). Interestingly, the cortical areas corresponding to the NFA appear as partially overlapping with those we show to represent numerosity along the ventral stream. Thus, according to this view, while a cortical patch in the ventral stream develops its response to number symbols, it concurrently increases its connectivity with the parietal regions encoding numerosity. This increased connectivity might cause numerosity representations to be broadcasted between parietal cortex and the NFA, such that both regions eventually come to represent both arabic digits and the associated numerosities (Piazza et al., 2007; Eger et al., 2009). Interestingly, and in line with this idea, a recent study performed on a few subjects and using the pRF approach indicated that neuronal populations tuned to small numerosity in the ventral occipitotemporal cortex region NTO also respond to arabic digits (Cai et al., 2023). This hypothesis predicts that the occipito-temporal response to numerosities may not be present in preschoolers, and that it develops as the effect of formal math education (Dehaene-Lambertz et al., 2018; Kersey et al., 2019). However, this hypothesis must be considered as highly tentative as the precise anatomical location of the NFA region remains rather poorly determined, and the precise relation between our NTO map encoding numerosity and the NFA as defined in a recent meta-analysis (Yeo et al., 2017) is only partial. Indeed, we do not know whether our ventral numerosity-responsive regions NTO would also encode digits, as we did not expose subjects to such stimuli.

Another possible interpretation, not necessarily exclusive with the first one, posits that both the dorsal and the ventral stream possess sufficient computational resources to independently represent numerosity, and that different representations of numerosity might serve different functional purposes. This view would also be in line with the finding that Convolutional Neural Networks (CNNs) trained on object categorization and well accounting for the brain activity in the human inferior

temporal cortex (Khaligh-Razavi & Kriegeskorte, 2014), contain, in their final layers, numerosity-tuned units, akin to monkey and human number neurons (Nasr et al., 2019). Interestingly, numerosity-tuned units were also found in an untrained CNN (Kim et al., 2021), suggesting that numerosity representations can emerge spontaneously based on mechanisms inherent to the visual system, independent from training. This hypothesis predicts that numerosity is represented in both streams independent from and prior to math education. These two hypotheses could be contrasted in the future by testing preschool children or innumerate adults.

In order to further explore the potential differences in numerosity representations across different brain regions, we further explored the neural representational geometry of our stimulus space using MDS, a hypothesis-free approach that may reveal some latent dimensions of the neural data that may otherwise remain invisible with a model-based approach such as RSA. When focussing on the topographically organized regions, we observed that the latent structure of the population level response in the early visual cortices (V1-V3) was characterized by a clear linear separation across numerosities as well as field areas, coherently with the RSA results indicating that in those areas not only number but also other visual features are well represented. Along the ventral stream, this linear manifold was also evident in the association ROIs hV4 and VO1, but it was progressively lost in the more anterior and medial regions VO2, PHC1 and PHC2, where no clear structure emerged, again coherently with the RSA results. Along the dorsal stream, the linear structure was replaced with a curved manifold in all IPS regions, yielding two orthogonal axes: one along which numerosities are ordered, and the other where the extreme numerosities are separated from the mid ones. Interestingly, such curved manifold was also clearly observed in non topographically organized areas in the ventro-lateral occipito-temporal areas highlighted in the searchlight analysis. The functional relevance of such a curved manifold remains currently unknown. Such bending of the “number line” imposed by the second dimension could represent the level of uncertainty that typically characterizes numerical or rank order judgements, whereby the extreme values are easier to evaluate and/or order compared to the middle ones. Interestingly, a recent CNN model specifically trained to perform a numerosity classification task developed an analogous curved structure in the last layer (Mistry et al., 2023), coherent with the idea that a curved manifold may be functionally relevant for comparative decision making. Indeed, a similar curved

structure bending around a midpoint from the MDS on BOLD data originating from the posterior parietal cortex was observed in a recent study while subjects engaged in a rank-ordering task (Nelli et al., 2023), suggesting that a similar neuronal schema may underlie both order and magnitude representations. The fact that this manifold encoding numerosity-related decision variables was observed in both parietal and occipito-temporal areas could indicate the presence of important functional connectivity between the dorsal and ventral pathways (Conrad et al., 2022), and it might be coherent with the idea that those regions, but not primary visual regions, host numerosity representations that are explicitly read out for numerical decisions making (Lasne et al., 2019; Moscoso et al., 2021). For example, Lasne et al. (2019) showed adult subjects visual set of different number of dots and observed that while numerosity could be equally well decoded by the BOLD activity in both early visual and parietal cortex, the inter-individual variability in numerosity comparison performance was solely predicted by decoding accuracy of the BOLD signal in parietal cortex. Currently, no studies investigated the behavioral relevance of the occipito-temporal representation of numerosity, thus this remains a question that future studies should resolve.

In summary, in this study we demonstrated that visual numerosity is represented beyond non-numerical visual features in a large set of regions, starting from early visual areas and further amplified along both the dorsal (up to anterior parietal) but also the ventral stream (up to the lateral and inferior occipito-temporal cortex), challenging the mainstream view of a preferential involvement of parietal cortex in numerosity representation (mainstream also reflected in the triple code model of numerical cognition (Dehaene and Cohen 1995; Dehaene et al., 2003). We also found that the neural representational geometry was identical across the dorsal and the ventral association areas, and substantially different from the one characterizing early numerosity representations in visual areas. The curved manifold present in both streams, whereby number is encoded together with decision variables, highlights the potential relevance for both dorsal and ventral associative regions for numerosity decision making.

Figures

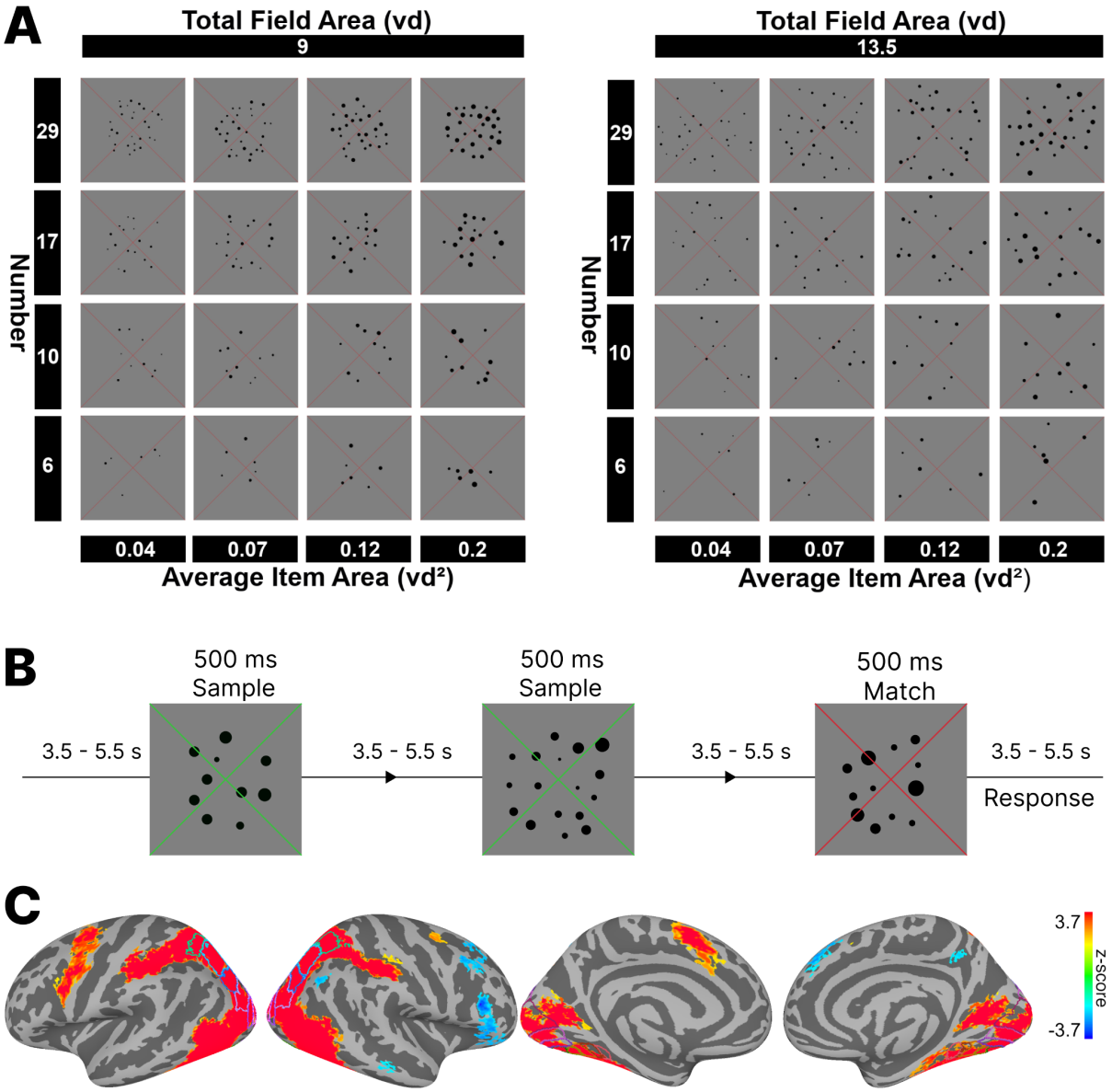

Figure 1. Stimulus set, design, and univariate effect of stimuli (A) Illustration of the stimulus conditions. Stimuli orthogonally varied in number (6,10,17,29), average item area (0.04, 0.07, 0.12 and 0.2 visual square degree), and total field area (9 and 13.5 visual degree). (B) Illustration of the temporal presentation of the stimuli during scanning. Participants were instructed to attend to the number of dots and keep the number in mind until the next set of dots was shown (after a variable time interval of 3.5–5.5 s). From time to time, the color of the fixation cross changed from red to green. When the color changed, subjects were required to compare the number of dots in the current set, (match stimulus), with the previous one (sample stimulus) by pressing a button. (C) Results obtained from the univariate surface-based group analysis (n = 31). The maps show the activation elicited for all sample stimuli contrasted against the implicit baseline. Activation maps are thresholded at $p < 0.01$, TFCE corrected, and displayed on Freesurfer's fsaverage surface with colored outlines identifying ROIs along the early visual areas (V1, V2, V3), the dorsal (V3AB, V7, IPS12, IPS345), and the ventral stream (hV4, VO1, VO2, PHC1, PHC2) from a surface-based probabilistic atlas (Wang et al., 2015).

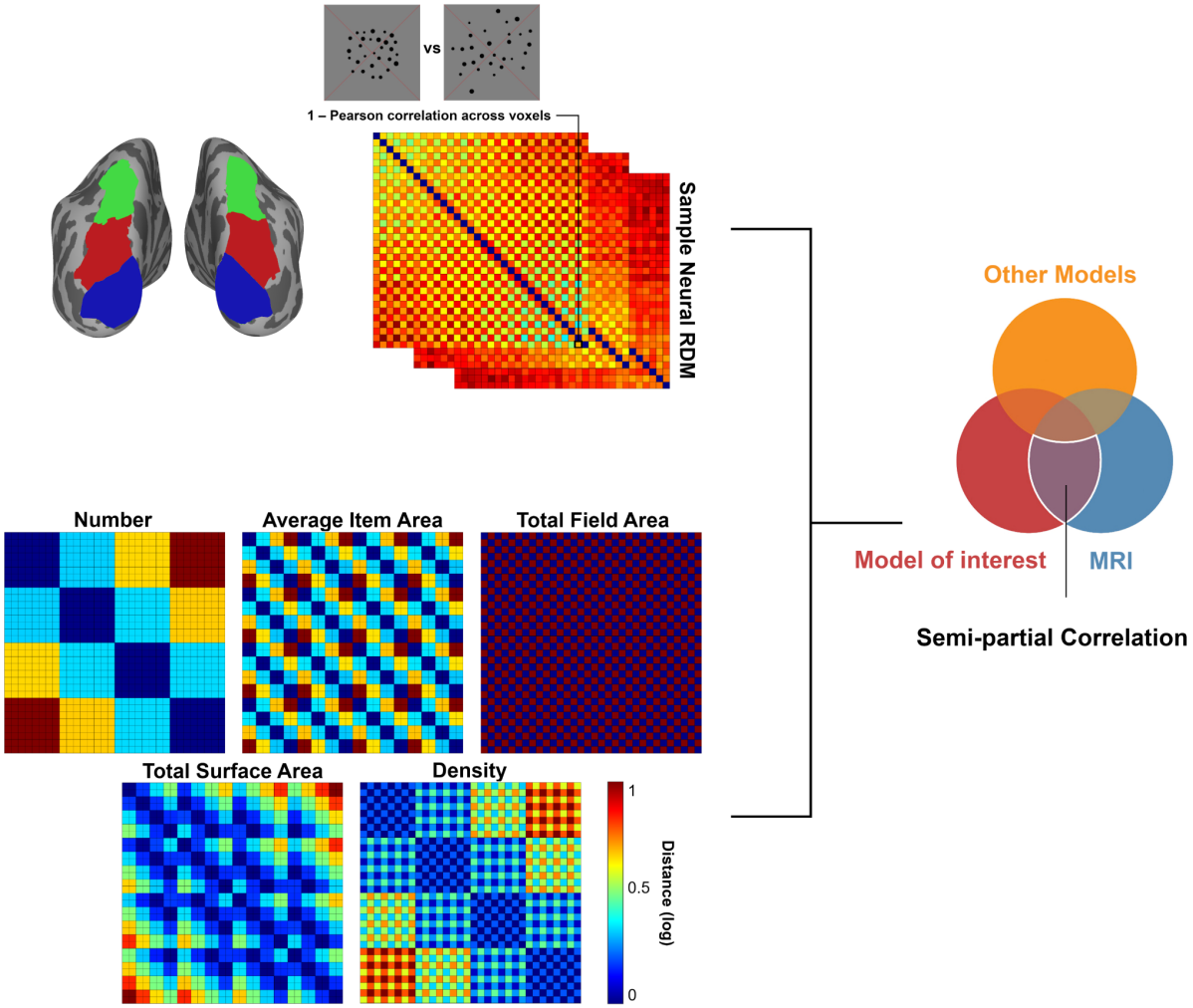

Figure 2. Neural representational dissimilarity matrices (RDM) derived from fMRI were entered into a semipartial correlation analysis. fMRI RDMs were created using 1 – Pearson correlation between the activations of voxels in that region for each pair of images. Five representational dissimilarity matrices, model RDMs, used as predictors in the semipartial correlation analysis. These matrices represent the logarithmic distance between pairs of stimuli in terms of number, average item area, total field area, total surface area, and density.

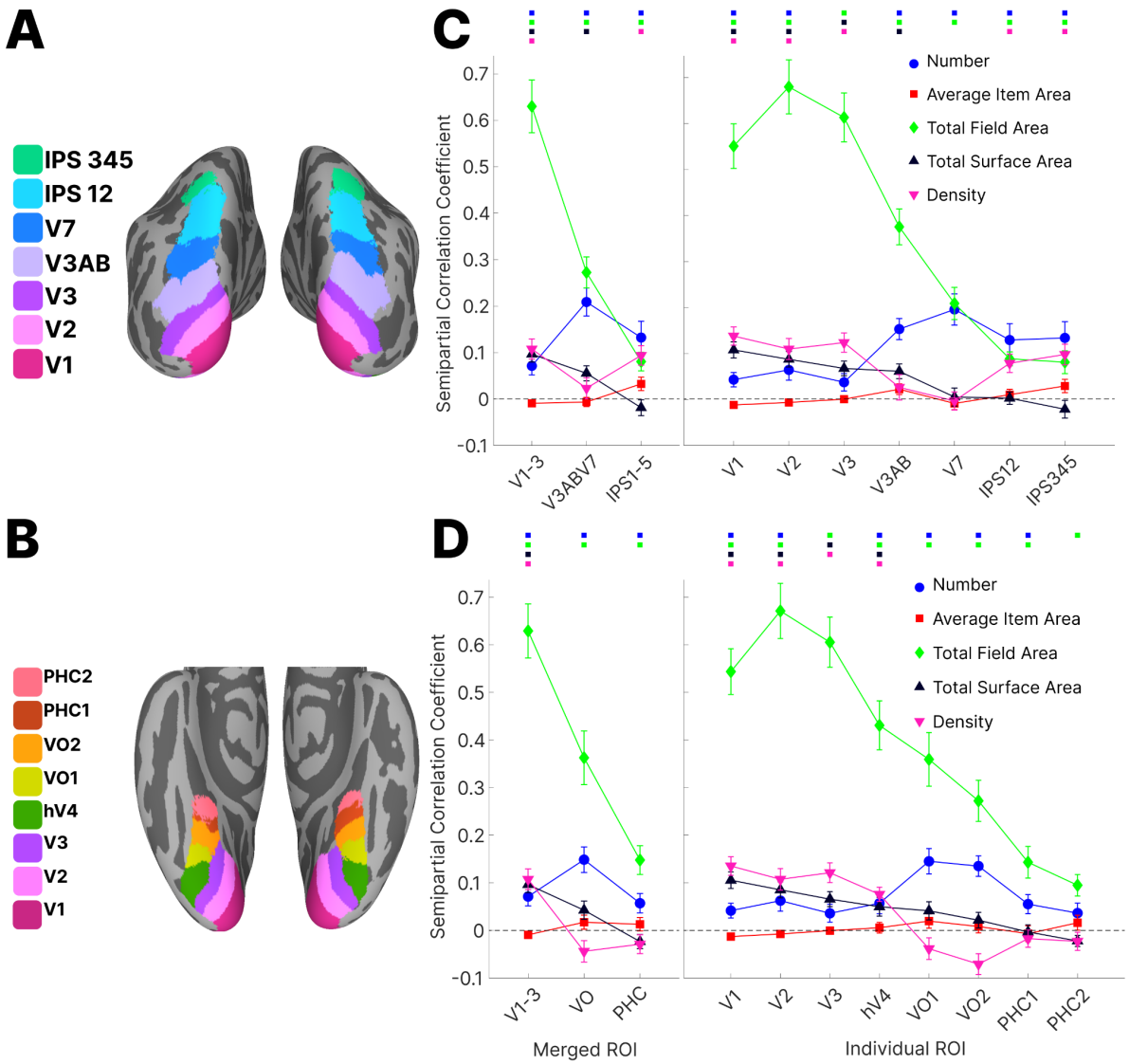

Figure 3. Color-coded ROIs for (A) dorsal and (B) ventral streams defined by the probabilistic atlas (Wang et al., 2015) are displayed on Freesurfer's fsaverage inflated surface. (C) Semipartial correlation coefficients obtained from the representational similarity analysis for number, average item area, total field area, total surface area and density from predefined dorsal retinotopic ROIs. Number is represented along other visual features in almost all regions and is amplified in association areas (from V3AB to IPS). Data points show mean semipartial correlation coefficients across subjects (n = 31) ± standard error of the mean (SEM). The coloured points above the figure indicate where the effect significantly exceeds zero ($p<0.01$). (D) Semipartial correlation coefficients obtained from the representational similarity analysis for number and all other features from predefined retinotopic ventral ROIs after normalizing with the corresponding noise ceiling. Note that the results from early visual areas V1-3 are the same across panels as the ventral and dorsal components of these areas were merged into a single ROI. Within the ventral stream, number is amplified in intermediate areas (VO1 and VO2). Data points show mean semipartial correlation coefficients across subjects (n = 31) ± standard error of the mean (SEM). The coloured points above the figure indicate where the effect significantly exceeds zero ($p<0.01$).

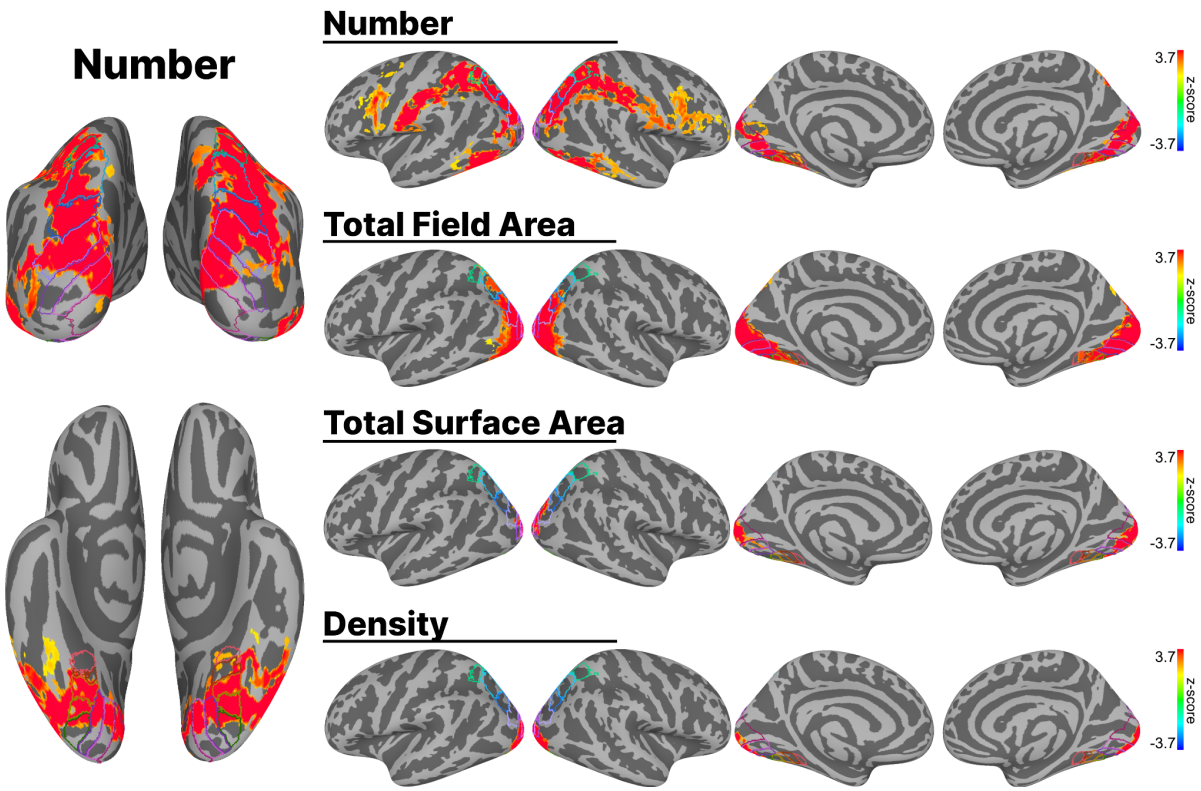

Figure 4. Surface-based searchlight representational similarity analysis searchlight (RSA) results obtained from the surface-based group analysis (n = 31). The maps show how patterns of activity across the cortical surface are captured by each model of interest (Number, Total Field Area, Total Surface Area, and Density) while partialling out the effect of other models. Activation maps are thresholded at $p < 0.01$, TFCE corrected, and displayed on Freesurfer's fsaverage surface with colored outlines identifying ROIs along the early visual (V1, V2, V3), the dorsal (V3AB, V7, IPS12, IPS345), and the ventral stream (hV4, VO1, VO2, PHC1, PHC2) from a surface-based probabilistic atlas (Wang et al., 2015).

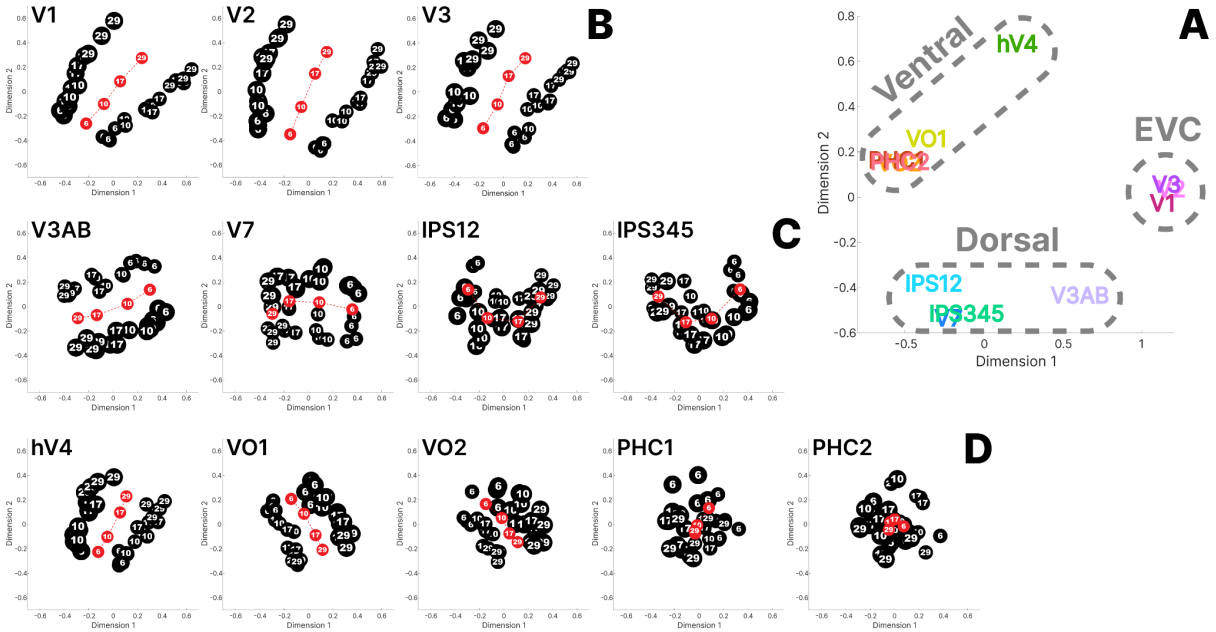

Figure 5. (A) Multidimensional scaling (MDS) reveals similarity of the representational structures between the predefined ROIs in a two-dimensional space. Here the proximity between any two ROIs indicates how similar their representation of the stimuli is. Three clusters of regions become apparent. MDS reveals representational similarities between stimuli in a two-dimensional space for regions in the (B) EVC, (C) dorsal regions, and (D) ventral regions. The black circles represent the 32 stimuli. They are labeled according to their numerosity (6, 10, 17, 29), and scaled in size to represent stimuli with small total field area (small circles) and larger total field area (large circles). The red circles indicate the average coordinates of each number.

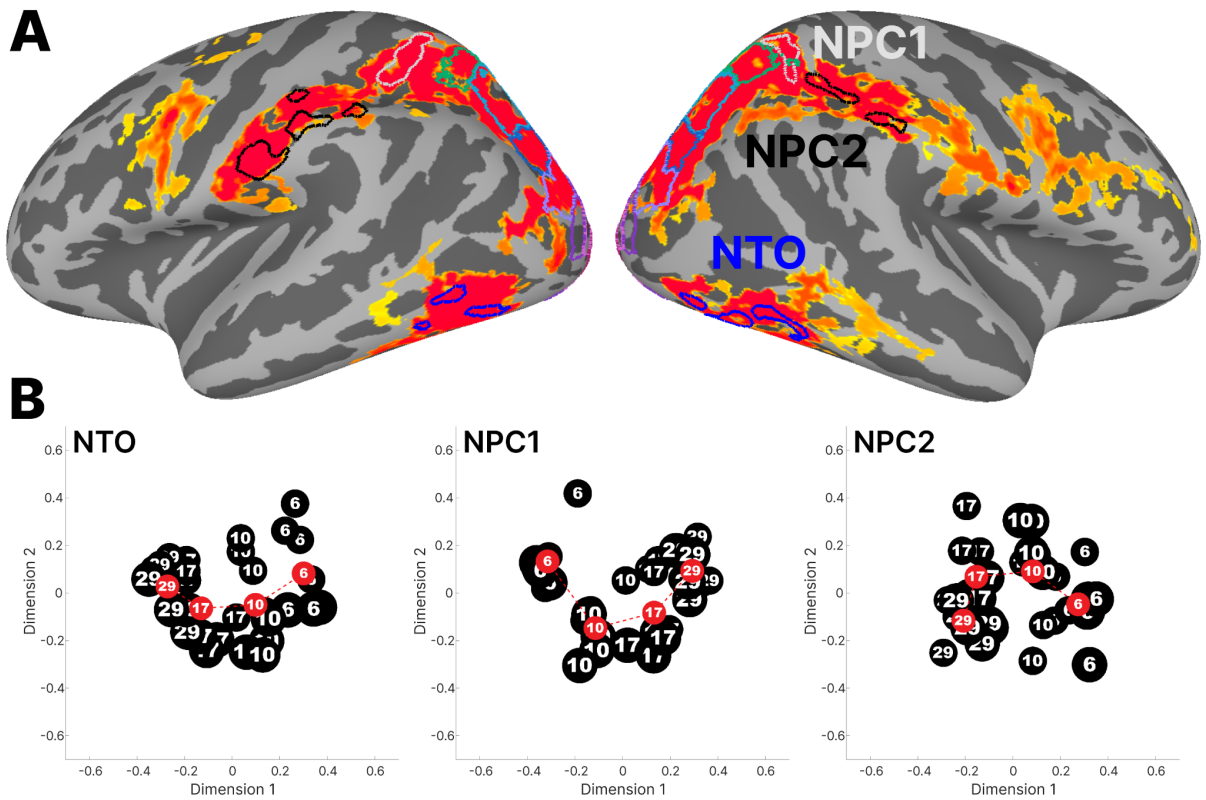

Figure 6. (A) ROIs (NTO, NPC1, NPC2) chosen using group-constrained subject-specific (GCSS) analysis from outside the retinotopic regions of interest, as defined in the probabilistic atlas by Wang et al. (2015), were visualized on the number activation map derived from the searchlight analysis. (B) Multidimensional scaling (MDS) reveals representational similarities between stimuli in a two-dimensional space for regions in the dorsal (NPC1, and NPC2) and the (C) ventral (NTO) stream.

References

Abdi, H. (2007). Part and partial correlations. In N. J. Salkind (Ed.), Encyclopedia of Measurement and Statistics (pp. 736–740).

Al-Tahan, H., & Mohsenzadeh, Y. (2021). Reconstructing feedback representations in the ventral visual pathway with a generative adversarial autoencoder. PLOS Computational Biology, 17(3), e1008775. https://doi.org/10.1371/journal.pcbi.1008775

Amalric, M., & Dehaene, S. (2016). Origins of the brain networks for advanced mathematics in expert mathematicians. Proceedings of the National Academy of Sciences of the United States of America, 113(18), 4909–4917. https://doi.org/10.1073/pnas.1603205113

Anobile, G., Cicchini, G. M., & Burr, D. (2013). Separate mechanisms for perception of numerosity and density. Psychological Science, 25(1), 265–270. https://doi.org/10.1177/0956797613501520

Ansari, D., & Dhital, B. (2006). Age-related Changes in the Activation of the Intraparietal Sulcus during Nonsymbolic Magnitude Processing: An Event-related Functional Magnetic Resonance Imaging Study. Journal of Cognitive Neuroscience, 18(11), 1820–1828. https://doi.org/10.1162/jocn.2006.18.11.1820

Behzadi, Y., Restom, K., Liau, J., & Liu, T. T. (2007). A component based noise correction method (CompCor) for BOLD and perfusion based fMRI. NeuroImage, 37(1), 90–101. https://doi.org/10.1016/j.neuroimage.2007.04.042

Brainard, D. H. (1997). The Psychophysics Toolbox. Spatial Vision, 10(4), 433–436. https://doi.org/10.1163/156856897x00357

Bulthé, J., de Smedt, B., & op de Beeck, H. (2014). Format-dependent representations of symbolic and non-symbolic numbers in the human cortex as revealed by multi-voxel pattern analyses. NeuroImage, 87, 311–322. https://doi.org/10.1016/j.neuroimage.2013.10.049

Bulthé, J., de Smedt, B., & op de Beeck, H. P. (2015). Visual Number Beats Abstract Numerical Magnitude: Format-dependent Representation of Arabic Digits and Dot Patterns in Human Parietal Cortex. Journal of Cognitive Neuroscience, 27(7), 1376–1387. https://doi.org/10.1162/jocn_a_00787

Burr, D., & Ross, J. (2008). A Visual Sense of Number. Current Biology, 18(6), 425–428. https://doi.org/10.1016/j.cub.2008.02.052

Burr, D., Anobile, G., & Arrighi, R. (2018). Psychophysical evidence for the number sense. Philosophical Transactions of the Royal Society B, 373(1740), 20170045. https://doi.org/10.1098/rstb.2017.0045

Cai, Y., Hofstetter, S., Van Dijk, J. A., Zuiderbaan, W., Van Der Zwaag, W., Harvey, B. M., & Dumoulin, S. O. (2021). Topographic numerosity maps cover subitizing and estimation ranges. Nature Communications, 12(1). https://doi.org/10.1038/s41467-021-23785-7

Cai, Y., Hofstetter, S., & Dumoulin, S. O. (2023). Nonsymbolic numerosity maps at the occipitotemporal cortex respond to symbolic numbers. The Journal of Neuroscience, 43(16), 2950–2959. https://doi.org/10.1523/jneurosci.0687-22.2023

Cantlon, J. F., Brannon, E. M., Carter, E., & Pelphrey, K. A. (2006). Functional imaging of numerical processing in adults and 4-y-Old children. *PLOS Biology*, *4*(5), e125. https://doi.org/10.1371/journal.pbio.0040125

Castaldi, E., Mirassou, A., Dehaene, S., Piazza, M., & Eger, E. (2018). Asymmetrical interference between number and item size perception provides evidence for a domain specific impairment in dyscalculia. PLOS ONE, 13(12), e0209256. https://doi.org/10.1371/journal.pone.0209256

Castaldi, E., Piazza, M., Dehaene, S., Vignaud, A., & Eger, E. (2019). Attentional amplification of neural codes for number independent of other quantities along the dorsal visual stream. ELife, 8. https://doi.org/10.7554/elife.45160

Castaldi E., Vignaud A., & Eger E. (2020). Mapping subcomponents of numerical cognition in relation to functional and anatomical landmarks of human parietal cortex. Neuroimage. 221:117210. https://doi.org/10.1016/j.neuroimage.2020.117210

Castelli, F., Glaser, D. E., & Butterworth, B. (2006). Discrete and analogue quantity processing in the parietal lobe: A functional MRI study. Proceedings of the National Academy of Sciences of the United States of America, 103(12), 4693–4698. https://doi.org/10.1073/pnas.0600444103

Chung, M. K., Robbins, S., Dalton, K. M., Davidson, R. J., Alexander, A. L., & Evans, A. C. (2005). Cortical thickness analysis in autism with heat kernel smoothing. NeuroImage, 25(4), 1256–1265. https://doi.org/10.1016/j.neuroimage.2004.12.052

Conrad, B., Pollack, C., Yeo, D. J., & Price, G. R. (2022). Structural and functional connectivity of the inferior temporal numeral area. Cerebral Cortex, 33(10), 6152–6170. https://doi.org/10.1093/cercor/bhac492

Cox, R. W. (1996). AFNI: Software for analysis and Visualization of Functional Magnetic Resonance neuroimages. Computers and Biomedical Research, 29(3), 162–173. https://doi.org/10.1006/cbmr.1996.0014

Decarli, G., Zingaro, D., Surian, L., & Piazza, M. (2023). Number sense at 12 months predicts 4-year-olds' maths skills. Developmental Science, 26(6). https://doi.org/10.1111/desc.13386

Dehaene-Lambertz, G., Monzalvo, K., & Dehaene, S. (2018). The emergence of the visual word form: Longitudinal evolution of category-specific ventral visual areas during reading acquisition. PLOS Biology, 16(3), e2004103. https://doi.org/10.1371/journal.pbio.2004103

Dehaene, S., & Cohen, L. (1995). Towards an anatomical and functional model of number processing. Mathematical Cognition, 1, 83–120.

Dehaene, S., Piazza, M., Pinel, P., & Cohen, L. (2003). Three parietal circuits for number processing. Cognitive Neuropsychology, 20(3–6), 487–506. https://doi.org/10.1080/02643290244000239

Ditz, H. M., & Nieder, A. (2016). Numerosity representations in crows obey the Weber–Fechner law. Proceedings of the Royal Society B: Biological Sciences, 283(1827), 20160083. https://doi.org/10.1098/rspb.2016.0083

Eger, E., Michel, V., Thirion, B., Amadon, A., Dehaene, S., & Kleinschmidt, A. (2009). Deciphering Cortical Number Coding from Human Brain Activity Patterns. Current Biology, 19(19), 1608–1615. https://doi.org/10.1016/j.cub.2009.08.047

Eger, E. (2016). Neuronal foundations of human numerical representations. Progress in Brain Research, 1–27. https://doi.org/10.1016/bs.pbr.2016.04.015

Faye, A., Jacquin-Courtois, S., Reynaud, E., Lesourd, M., Besnard, J., & Osiurak, F. (2019). Numerical cognition: A meta-analysis of neuroimaging, transcranial magnetic stimulation and brain-damaged patients studies. NeuroImage: Clinical, 24, 102053. https://doi.org/10.1016/j.nicl.2019.102053

Fedorenko, E., Hsieh, P., Nieto-Castañón, A., Whitfield-Gabrieli, S., & Kanwisher, N. (2010). New method for FMRI investigations of language: defining ROIS functionally in individual subjects. Journal of Neurophysiology, 104(2), 1177–1194. https://doi.org/10.1152/jn.00032.2010

Fischl, B. (2012). FreeSurfer. NeuroImage, 62(2), 774–781. https://doi.org/10.1016/j.neuroimage.2012.01.021

Gallistel, C. R., & Gelman, R. (1992). Preverbal and verbal counting and computation. Cognition, 44(1–2), 43–74. https://doi.org/10.1016/0010-0277(92)90050-r

Gebuis, T., Gevers, W., & Kadosh, R. C. (2014). Topographic representation of high-level cognition: numerosity or sensory processing? Trends in Cognitive Sciences, 18(1), 1–3. https://doi.org/10.1016/j.tics.2013.10.002

Grotheer, M., Jeska, B., & Grill-Spector, K. (2018). A preference for mathematical processing outweighs the selectivity for Arabic numbers in the inferior temporal gyrus. NeuroImage, 175, 188–200. https://doi.org/10.1016/j.neuroimage.2018.03.064

Harvey, B. M., Klein, B. P., Petridou, N., & Dumoulin, S. O. (2013). Topographic Representation of Numerosity in the Human Parietal Cortex. Science, 341(6150), 1123–1126. https://doi.org/10.1126/science.1239052

Harvey, B. M., & Dumoulin, S. O. (2017). A network of topographic numerosity maps in human association cortex. Nature Human Behaviour, 1(2). https://doi.org/10.1038/s41562-016-0036

Halberda, J., Mazzocco, M. M., & Feigenson, L. (2008). Individual differences in non-verbal number acuity correlate with maths achievement. Nature, 455(7213), 665–668. https://doi.org/10.1038/nature07246

Hyde, D. C., Boas, D. A., Blair, C., & Carey, S. (2010). Near-infrared spectroscopy shows right parietal specialization for number in pre-verbal infants. NeuroImage, 53(2), 647–652. https://doi.org/10.1016/j.neuroimage.2010.06.030

Izard, V., Dehaene-Lambertz, G., & Dehaene, S. (2008). Distinct cerebral pathways for object identity and number in human infants. PLOS Biology, 6(2), e11. https://doi.org/10.1371/journal.pbio.0060011

Julian, J. B., Fedorenko, E., Webster, J., & Kanwisher, N. (2012). An algorithmic method for functionally defining regions of interest in the ventral visual pathway. NeuroImage, 60(4), 2357–2364. https://doi.org/10.1016/j.neuroimage.2012.02.055

Kasper, L., Bollmann, S., Diaconescu, A. O., Hutton, C., Heinzle, J., Iglesias, S., Hauser, T. U., Sebold, M., Manjaly, Z., Pruessmann, K. P., & Stephan, K. E. (2017). The PhysIO toolbox for modeling physiological noise in FMRI data. Journal of Neuroscience Methods, 276, 56–72. https://doi.org/10.1016/j.jneumeth.2016.10.019

Kay, K., & Yeatman, J. D. (2017). Bottom-up and top-down computations in word- and face-selective cortex. eLife, 6. https://doi.org/10.7554/elife.22341

Kersey, A. J., Wakim, K., Li, R., & Cantlon, J. F. (2019). Developing, mature, and unique functions of the child's brain in reading and mathematics. Developmental Cognitive Neuroscience, 39, 100684. https://doi.org/10.1016/j.dcn.2019.100684

Kim, G., Jang, J., Baek, S., Song, M., & Paik, S. B. (2021). Visual number sense in untrained deep neural networks. Science Advances, 7(1), eabd6127. https://doi.org/10.1126/sciadv.abd6127

Khaligh-Razavi, S., & Kriegeskorte, N. (2014). Deep Supervised, but Not Unsupervised, Models May Explain IT Cortical Representation. *PLOS Computational Biology*, *10*(11), e1003915. https://doi.org/10.1371/journal.pcbi.1003915

Khaligh-Razavi, S., Cichy, R. M., Pantazis, D., & Oliva, A. (2018). Tracking the spatiotemporal neural dynamics of real-world object size and animacy in the human brain. Journal of Cognitive Neuroscience, 30(11), 1559–1576. https://doi.org/10.1162/jocn_a_01290

Kobylkov, D., Mayer, U., Zanon, M., & Vallortigara, G. (2022). Number neurons in the nidopallium of young domestic chicks. Proceedings of the National Academy of Sciences of the United States of America, 119(32). https://doi.org/10.1073/pnas.2201039119

Kriegeskorte, N., Mur, M., & Bandettini, P. A. (2008). Representational similarity analysis – connecting the branches of systems neuroscience. Frontiers in Systems Neuroscience. https://doi.org/10.3389/neuro.06.004.2008

Kriegeskorte, N., & Kievit, R. A. (2013). Representational geometry: integrating cognition, computation, and the brain. Trends in Cognitive Sciences, 17(8), 401–412. https://doi.org/10.1016/j.tics.2013.06.007

Kruskal, J. B. (1964). Multidimensional scaling by optimizing goodness of fit to a nonmetric hypothesis. Psychometrika, 29(1), 1–27. https://doi.org/10.1007/bf02289565

Kutter, E. F., Bostroem, J., Elger, C. E., Mormann, F., & Nieder, A. (2018). Single neurons in the human brain encode numbers. Neuron, 100(3), 753-761.e4. https://doi.org/10.1016/j.neuron.2018.08.036

Kutter, E. F., Boström, J., Elger, C. E., Nieder, A., & Mormann, F. (2022). Neuronal codes for arithmetic rule processing in the human brain. Current Biology, 32(6), 1275-1284.e4. https://doi.org/10.1016/j.cub.2022.01.054

Kutter, E. F., Dehnen, G., Borger, V., Surges, R., Mormann, F., & Nieder, A. (2023). Distinct neuronal representation of small and large numbers in the human medial

temporal lobe. Nature Human Behaviour. https://doi.org/10.1038/s41562-023-01709-3\

Lasne, G., Piazza, M., Dehaene, S., Kleinschmidt, A., & Eger, E. (2019). Discriminability of numerosity-evoked fMRI activity patterns in human intra-parietal cortex reflects behavioral numerical acuity. Cortex, 114, 90–101. https://doi.org/10.1016/j.cortex.2018.03.008

Lemer, C., Dehaene, S., Spelke, E. S., & Cohen, L. (2003). Approximate quantities and exact number words: dissociable systems. Neuropsychologia, 41(14), 1942–1958. https://doi.org/10.1016/s0028-3932(03)00123-4

Merten, K., & Nieder, A. (2009). Compressed scaling of abstract numerosity representations in adult humans and monkeys. Journal of Cognitive Neuroscience, 21(2), 333–346. https://doi.org/10.1162/jocn.2008.21032

Mistry, P. K., Strock, A., Liu, R., Young, G. B., & Menon, V. (2023). Learning-induced reorganization of number neurons and emergence of numerical representations in a biologically inspired neural network. Nature Communications, 14(1). https://doi.org/10.1038/s41467-023-39548-5

Mitchell, T. M., Hutchinson, R., Niculescu, R. S., Pereira, F., Wang, X., Just, M. A., & Newman, S. D. (2004). Learning to Decode Cognitive States from Brain Images. Machine Learning, 57(1/2), 145–175. https://doi.org/10.1023/b:mach.0000035475.85309.1b

Moeller, S., Yacoub, E., Olman, C. A., Auerbach, E. J., Strupp, J., Harel, N., & Uğurbil, K. (2010). Multiband multislice GE-EPI at 7 tesla, with 16-fold acceleration using partial parallel imaging with application to high spatial and temporal whole-brain fMRI. Magnetic Resonance in Medicine, 63(5), 1144–1153. https://doi.org/10.1002/mrm.22361

Moscoso, P. a. M., Greenlee, M. W., Anobile, G., Arrighi, R., Burr, D., & Castaldi, E. (2021). Groupitizing modifies neural coding of numerosity. Human Brain Mapping, 43(3), 915–928. https://doi.org/10.1002/hbm.25694

Nasr, K., Viswanathan, P., & Nieder, A. (2019). Number detectors spontaneously emerge in a deep neural network designed for visual object recognition. Science Advances, 5(5), eaav7903. https://doi.org/10.1126/sciadv.aav7903

Nelli, S., Braun, L., Dumbalska, T., Saxe, A. M., & Summerfield, C. (2023). Neural knowledge assembly in humans and neural networks. Neuron, 111(9), 1504-1516.e9. https://doi.org/10.1016/j.neuron.2023.02.014

Nieder, A., & Miller, E. K. (2003). Coding of Cognitive Magnitude. Neuron, 37(1), 149–157. https://doi.org/10.1016/s0896-6273(02)01144-3

Nieder, A., & Miller, E. K. (2004). A parieto-frontal network for visual numerical information in the monkey. Proceedings of the National Academy of Sciences of the United States of America, 101(19), 7457–7462. https://doi.org/10.1073/pnas.0402239101

Nieder, A. (2020). The Adaptive Value of Numerical Competence. Trends in Ecology & Evolution, 35(7), 605–617. https://doi.org/10.1016/j.tree.2020.02.009

Nieto-Castañón, A., & Fedorenko, E. (2012). Subject-specific functional localizers increase sensitivity and functional resolution of multi-subject analyses. NeuroImage, 63(3), 1646–1669. https://doi.org/10.1016/j.neuroimage.2012.06.065

Nili, H., Wingfield, C., Walther, A., Su, L., Marslen-Wilson, W. D., & Kriegeskorte, N. (2014). A toolbox for representational similarity analysis. PLOS Computational Biology, 10(4), e1003553. https://doi.org/10.1371/journal.pcbi.1003553

Oosterhof, N. N., Wiestler, T., Downing, P. E., & Diedrichsen, J. (2011). A comparison of volume-based and surface-based multi-voxel pattern analysis. NeuroImage, 56(2), 593–600. https://doi.org/10.1016/j.neuroimage.2010.04.270

Oosterhof, N. N., Connolly, A. C., & Haxby, J. V. (2016). COSMOMVPA: Multi-Modal Multivariate Pattern Analysis of Neuroimaging data in Matlab/GNU Octave. Frontiers in Neuroinformatics, 10. https://doi.org/10.3389/fninf.2016.00027

Piantadosi, S. T., & Cantlon, J. F. (2017). True numerical cognition in the wild. Psychological Science, 28(4), 462–469. https://doi.org/10.1177/0956797616686862

Piazza, M., Izard, V., Pinel, P., le Bihan, D., & Dehaene, S. (2004). Tuning Curves for Approximate Numerosity in the Human Intraparietal Sulcus. Neuron, 44(3), 547–555. https://doi.org/10.1016/j.neuron.2004.10.014

Piazza, M., Pinel, P., le Bihan, D., & Dehaene, S. (2007). A Magnitude Code Common to Numerosities and Number Symbols in Human Intraparietal Cortex. Neuron, 53(2), 293–305. https://doi.org/10.1016/j.neuron.2006.11.022

Piazza, M. (2010). Neurocognitive start-up tools for symbolic number representations. Trends in Cognitive Sciences, 14(12), 542–551. https://doi.org/10.1016/j.tics.2010.09.008

Piazza, M., & Eger, E. (2016). Neural foundations and functional specificity of number representations. Neuropsychologia, 83, 257–273. https://doi.org/10.1016/j.neuropsychologia.2015.09.025

Revkin, S. K., Piazza, M., Izard, V., Cohen, L., & Dehaene, S. (2008). Does subitizing reflect numerical estimation? Psychological Science, 19(6), 607–614. https://doi.org/10.1111/j.1467-9280.2008.02130.x

Rosenke, M., Van Hoof, R., Van Den Hurk, J., Grill-Spector, K., & Goebel, R. (2020). A Probabilistic Functional Atlas of Human Occipito-Temporal Visual Cortex. *Cerebral Cortex*, *31*(1), 603–619. https://doi.org/10.1093/cercor/bhaa246

Saad, Z. S., Reynolds, R. C., Argall, B., Japee, S., & Cox, R. W. (2005). SUMA: An interface for surface-based intra- and inter-subject analysis with AFNI. IEEE International Symposium on Biomedical Imaging: From Nano to Macro. https://doi.org/10.1109/isbi.2004.1398837

Scott, T. L., & Perrachione, T. K. (2019). Common cortical architectures for phonological working memory identified in individual brains. NeuroImage, 202, 116096. https://doi.org/10.1016/j.neuroimage.2019.116096

Smith, S. M., & Nichols, T. E. (2009). Threshold-free cluster enhancement: Addressing problems of smoothing, threshold dependence and localisation in cluster inference. NeuroImage, 44(1), 83–98. https://doi.org/10.1016/j.neuroimage.2008.03.061

Wagener, L., Loconsole, M., Ditz, H. M., & Nieder, A. (2018). Neurons in the Endbrain of Numerically Naive Crows Spontaneously Encode Visual Numerosity. Current Biology, 28(7), 1090–1094.e4. https://doi.org/10.1016/j.cub.2018.02.023

Wang, L., Mruczek, R. E. B., Arcaro, M., & Kästner, S. (2014). Probabilistic maps of visual topography in human cortex. Cerebral Cortex, 25(10), 3911–3931. https://doi.org/10.1093/cercor/bhu277

Warrington, E. K., & James, M. (1967). Tachistoscopic number estimation in patients with unilateral cerebral lesions. Journal of Neurology, Neurosurgery, and Psychiatry, 30(5), 468–474. https://doi.org/10.1136/jnnp.30.5.468

Yeo, D. J., Wilkey, E. D., & Price, G. R. (2017). The search for the number form area: A functional neuroimaging meta-analysis. Neuroscience & Biobehavioral Reviews, 78, 145–160. https://doi.org/10.1016/j.neubiorev.2017.04.027